Cement & Concrete Composites 33 (2011) 814–823

Contents lists available at ScienceDirect

Cement & Concrete Composites

journal homepage: www.elsevier.com/locate/cemconcomp

Effect of fiber shape and morphology on interfacial bond and cracking behaviors of sisal fiber cement based composites

Flávio de Andrade Silva [a], Barzin Mobasher [c,*], Chote Soranakom [b], Romildo Dias Toledo Filho [a]

[a] Civil Engineering Department, COPPE, Universidade Federal do Rio de Janeiro, P.O. Box 68506, CEP 21941-972 Rio de Janeiro, RJ, Brazil
[b] Infrastructure Monitoring and Management System (IMMS Co., Ltd.), Bangkok, Thailand
[c] School of Sustainable Engineering and the Built Environment, Arizona State University, Tempe, AZ, USA

ARTICLE INFO

Article history:
Received 10 November 2010
Received in revised form 9 May 2011
Accepted 9 May 2011
Available online 18 May 2011

Keywords:
Natural fibers
Sisal
Pull-out
Interface
Cement based composites

ABSTRACT

An experimental investigation was performed to understand the pull-out behavior of sisal fibers from a cement matrix. The effect of curing age and fiber embedment length on the fiber–matrix interface was studied. Sisal fiber presents irregular cross-section with different shapes that may be beneficial for the bond strength. A scanning electron microscope coupled with image analysis was used to measure the cross-section area of individual tested fibers and to determine and classify their morphology. The results were correlated to the fiber morphology. Direct tension tests were performed on composites reinforced by 10% in volume of continuous aligned sisal fiber. A finite difference model developed earlier by authors was used to determine the bond strength versus slip constitutive relation from experimental data and to predict the composite tensile behavior and crack spacing. It was found that the sisal fiber morphology plays an important role in the bond strength. Average adhesional bond strength as high as 0.92 MPa were reported for the fiber shape that promoted the best interfacial performance.

1. Introduction

Cement based composites reinforced with continuous aligned sisal fibers demonstrate a tension-hardening with multiple cracking behavior [1] with high tolerance to fatigue loading [2] and high energy absorption capacity under dynamic loading [3]. This type of composite system is reinforced with up to five layers of fibers resulting in a total volume fraction of 10%. In humid environments the sisal fiber cement composites produced with ordinary Portland cement matrices undergo an aging process during which they may suffer a reduction in post-cracking strength and toughness. This process is a result of migration of hydration products (mainly $Ca(OH)_2$) to the fiber structure. To mitigate this effect a special matrix that has 50% of cement replaced by calcined clays has been recently developed and optimized for use with sisal fiber systems [4]. This matrix lowers the calcium hydroxide production resulting in enhanced durability against fiber degradation and also providing adequate rheology in the fresh state for the fiber volume fractions proposed. The multiple cracking behavior achieved is governed by interfacial bond characteristics between fiber and matrix.

A significant amount of experimental and analytical investigations have been dedicated to the mechanical characterization of interface in man-made-fiber cement matrix systems. Tests for bond adhesion of cementitious composites have been performed by many researchers; however, limited data has been presented for natural fibers. Most of the interface characterization work has been performed on steel, glass and polymeric fibers. Naaman and Najm [5] state that there are four main factors that influence the bond between fiber and matrix: (i) physical and chemical adhesion, (ii) mechanical component of bond such as deformed, crimped and hooked end fibers, (iii) fiber-to-fiber interlock, and (iv) friction. Peled and Bentur [6] investigated the pull-out behavior of straight and crimped polyethylene yarns. They found that increasing the crimp density enhances the mechanical anchoring and the equivalent adhesion bond strength increases from 1 to 1.84 MPa (10 mm fiber embedded length). Markovich et al. [7] studied the pull-out behavior of hooked end steel fibers for different types of matrices and reported an average frictional stress between 2.76 and 4.97 MPa depending on the mixture. Kim et al. [8] investigated steel hooked ended and torroidal shaped fibers. Equivalent bond stresses calculated from experimental pull-out of hooked end and torroidal fibers were 4.7 and 14.5 MPa, respectively.

Several models have been used for prediction and characterization of pull-out behavior in fiber reinforced cement composites. Naaman et al. [9] proposed an analytical model for smooth fibers or bars with an idealized bond–stress–slip relationship of the interface. The solution led to the prediction of the bond shear stress-versus slip curve assuming that one can employ a back-calculation procedure to use the pull-out load versus slip in

* Corresponding author. Tel.: +1 480 965 0141; fax: +1 480 965 0557.
E-mail address: barzin@asu.edu (B. Mobasher).

0958-9465/$ - see front matter © 2011 Elsevier Ltd. All rights reserved.
doi:10.1016/j.cemconcomp.2011.05.003

parameter estimation. Sueki et al. [10] modified Naaman's model to analyze pull-out test results and quantified the equivalent bond properties of several fabrics. In their analysis, the role of fill yarns in providing anchorage points along the length were modeled in a discrete approach. Banholzer et al. [11] proposed another analytical model to simulate the pull-out response of a fiber–matrix system in which an N-piecewise linear bond stress versus slip relation is adopted.

In the present research single fiber pull-out tests were performed on sisal fibers for curing ages ranging from 3 to 28 days. Embedment lengths of 10, 20, 30 and 40 mm were tested for samples after 3 days of curing. Microstructure characterization was coupled with image analysis in order to compute the sisal fiber area of each test and to investigate the effect of the fiber shape on the bond strength. A non-linear finite difference model developed by Soranakom and Mobasher [12–14] for a regularly anchored, and aligned fiber composite was used to simulate the pull-out response. The pull-out results were then used in predicting direct tensile and crack spacing of sisal fiber reinforced composites based on the interface properties. The numerical analysis is compared to experiments, and it is shown that small modifications to the model are necessary in order to fit the response of unidirectional aligned fibers.

2. Experimental program

2.1. Materials and processing

The sisal fibers used in this investigation were extracted from the sisal plant farm located in the city of Valente, state of Bahia – Brazil. Their mechanical properties consisted of a mean elastic modulus and tensile strength of 19 GPa and 400 MPa, respectively as characterized by Silva et al. [15]. More information on the mechanical properties of the used sisal fiber can be obtained elsewhere [16,17].

The matrix used in the present work was based on past research [4,18]. It was produced using the Portland cement CPII F-32, river sand with maximum diameter of 1.18 mm and density of 2.67 g/cm^3, 5% in volume of wollastonite (JG class) as micro reinforcement and a naphthalene superplasticizer Fosroc Reax Conplast SP 430 with content of solids of 44%. The use of micro-fiber reinforcement was directed at increasing the matrix tensile strength and to adjust the matrix rheology. Metakaolin (MK) from Metacaulim do Brasil Industria e Comércio Ltda and calcined waste crushed clay brick (CWCCB) obtained from an industry located in Itaborai – RJ, Brazil, burned at 850 °C, were used as cement replacements. The cement was replaced by 30% of MK and 20% of CWCCB following previous studies [4,18]. The mortar matrix had a mix design of 1:1:0.4 (cementitious material:sand:water) by weight.

The matrix was produced using a bench-mounted mechanical mixer of 5 l capacity. The cementitious materials, sand and wollastonite fibers were dry mixed during 5 min (for homogenization). Water and superplasticizer were slowly added in and the mixture was blended for 5 min. Molds were designed for casting single filament pull-out specimens (see Fig. 1). PVC tubes were used as the formwork while wooden bases were used to guarantee the accuracy of the sisal fiber orientation at the centroidal axis of the mold through a hole drilled at the center of the base plate. The sisal fiber was inserted through the eye of a needle, which was then contrived through the wooden mold. The mix was then poured into the PVC tubes in three layers followed by manual compaction. The specimens were covered in their molds for 24 h and after this time they were demolded and cured in water. Tensile specimens with a volume fraction of 10% continuous aligned sisal fibers were manufactured using the same mixture design [1].

2.2. Testing

2.2.1. Single fiber pull-out tests

An electromechanical MTS (model SINTECH 1/S) was used for the pull-out tests. The test setup is shown in Fig. 2. The PVC mold (diameter of 25 mm) was connected to a 0.44 kN (100 lb) load cell that was attached to the crosshead. The bottom part consisted of a pinch grip where the free end of the fiber was tightened. The test was conducted under constant crosshead displacement control at a rate of 0.1 mm/min. Six specimens of embedment length ranging

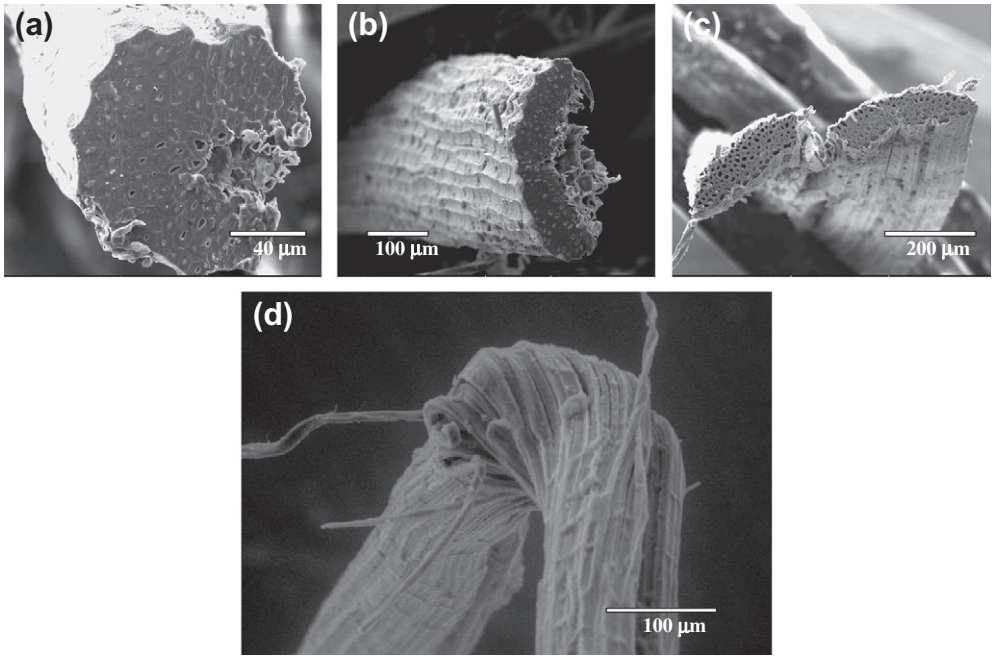

Fig. 1. Different morphologies of the sisal fiber: (a) horse-shoe shape, (b) arch shape, and (c) twisted arch shape. The different type of morphologies affects the fiber–matrix bond strength. The rough surface and flexibility of the fiber is observed in (d).

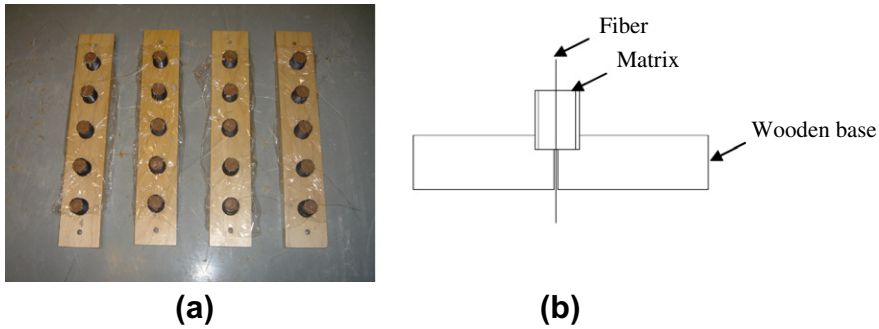

Fig. 2. Molds for casting pullout specimens: (a) picture of four of the molds and (b) schematic drawing showing the alignment of the fiber.

from 10 to 40 mm were tested after 3 days of curing. To investigate the influence of curing age on the fiber–matrix bond strength specimens with embedment length of 20 mm were tested at ages ranging from 3 to 28 days.

2.2.2. Direct tension tests in sisal fiber reinforced composite

Direct tensile tests were performed in an Instron servo hydraulic universal testing machine with a capacity of 500 kN. The tests were controlled by the cross-head displacement at a rate of 0.1 mm/min. Six specimens measuring 400 mm × 50 mm × 12 mm (length × width × thickness) were tested using a gage length of 300 mm with fixed–fixed boundary conditions. Aluminum thin sheets were glued on both ends of the specimen and the pressure of the hydraulic grips was adjusted to 1.37 MPa (200 psi) in order to minimize stress concentration and damage. Tensile strains were measured by a strain gage glued on the center of the specimen, and results were compared with the nominal strain values obtained from the stroke displacement. The tensile load, cross head displacement and strain were recorded by means of digital data acquisition.

Crack spacing during the tensile tests was measure by image analysis and correlated to strain following the procedure described elsewhere [1].

2.2.3. Microstructure

The sisal fiber's microstructure was investigated using an Environmental SEM (Philips FEI-XL 30). The scanning electron microscopy was under low vacuum chamber to remove the high vacuum constraint in the sample environment. The microscope was operated under an accelerating voltage ranging from 10 kV to 20 kV. No precoating with carbon or gold, as is done for standard high vacuum SEM, was required. The specimen chamber pressure was adjusted to values ranging from 25 to 80 Pa.

In order to measure the fiber's cross-sectional area, for each single fiber pull-out test, an adjacent piece of the fiber (immediately next to the one tested) was kept for future measurement and morphology characterization using the SEM. The obtained images were post-processed using ImageJ, a Java-based image processing program.

3. Results and discussion

Natural sisal fibers present non-regular cross sectional geometry (see Fig. 3) which enhances their bond characteristics. Similar irregular cross-sections were also reported for fique fibers [19]. These shape and geometrical changes results in a wide range of values obtained when mechanical bond parameters are measured. The general cross section of the fibers can be distinguished into three types of shapes that alter the interfacial mechanical response: (i) horse-shoe shape – located in the periphery of the leaf, these represents the majority of the fibers that can be found in the sisal plant (see Fig. 3a); (ii) arched shape – located in the center part of the sisal leaf in a lower proportion than the horse-shoe shape (see Fig. 3b); (iii) twisted arch shape – that is a result of the fiber extraction process (see Fig. 3c). The sisal fibers are extracted from its leaf by a mechanical process. In this process, it is potentially possible for some arch shaped fibers to break and twist, thus resulting in the type (iii) shape. In addition to these shapes of the sisal fibers, there are possibilities of formation of corrugated

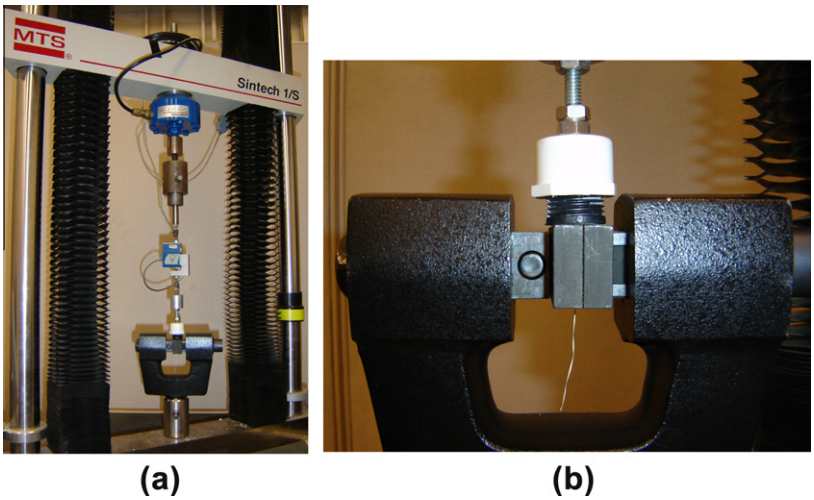

Fig. 3. Details of pullout test set-up: (a) MTS Sintech machine and (b) detail of grips.

surfaces and/or random variations along the fiber length which help the anchorage process. Virtually all the variations in fibers geometrical shape are beneficial to the fiber–matrix adhesion. When used as continuous reinforcement in cement matrices, the enhanced mechanical bond strength presented by the sisal fiber combined with its high tensile strength results in a composite with strain hardening and multiple cracking behavior under direct tensile load as presented in Fig. 4.

Most of the tension stiffening (ability of the uncracked segments in between the two parallel cracks to carry tensile force) models presented in the literature either does not take into account the bond–slip mechanism or simplifies it to a linear interfacial model. The Soranakom and Mobasher's model [12–14] is based on finite difference method, takes into account non-linear bond slip model and has options for inserting anchorage ribs to integrate the effect of crossing yarns. The anchorage options were not used in the present model. The cracking criterion and constitutive materials equation are illustrated in Fig. 5 and present a schematic drawing of a continuous sisal fiber reinforced composite defined by three distinct mechanisms: matrix strength cracking criterion, interface bond–slip characteristics and tensile stress–strain of the continuous fibers.

The first criterion is the cracking strength of matrix, $\sigma_{m,cr}$, as shown in Fig. 5a. A uniform or probabilistic strength distribution can be generated along the length of specimen by an appropriate probability density function (PDF) to result in deterministic or stochastic crack evolution in the specimen. The matrix at the grips is strengthened by metal plates and cracking is prohibited in these regions. The crack detection algorithm ignores the possibility of stress exceeding cracking strength at the grips.

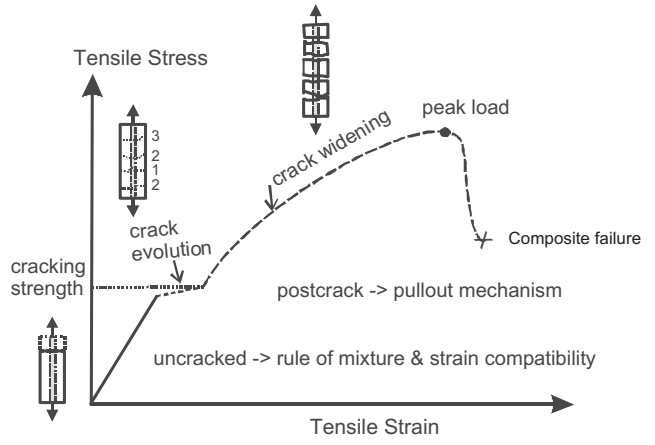

Fig. 4. Schematic drawing of the tensile response of a continuous sisal fiber cement based composite.

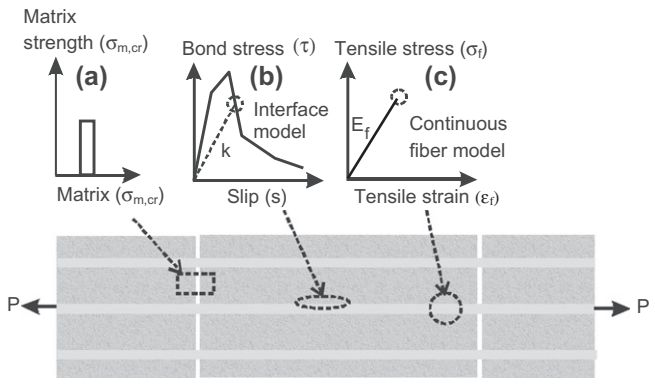

Fig. 5. Schematic drawing of a continuous sisal fiber reinforced composite, defined by three distinct mechanisms: (a) matrix strength cracking criterion, (b) interface bond–slip characteristics, and (c) tensile stress–strain of the continuous fibers.

The second modeling aspect is the bond between fiber and matrix, which is described by a generalized free form bond stress $\tau = \tau(s)$ expressed as function of slip (s) (Fig. 5b). Several linear segments define the pre and post-peak behaviors of the bond characteristics. At each load step, a secant modulus k enforces the local bond stress and slip at each node in the finite difference model to follow the prescribed bond–slip relation.

The third aspect (Fig. 5c), fiber properties, was simplified from the original model since the present work addressed continuous fibers instead of 2-D fabrics. The fiber mechanical properties were determined in a previous work [15].

The tension stiffening model [13,14] is based on equilibrium equations of the nodes. The equations are expressed as coefficient and the unknown variable slip (s), defined as the relative difference between the elongation of the continuous fibers and matrix:

$$s = \int_{x_i}^{x_{i+1}} (\varepsilon_y - \varepsilon_m) dx \tag{1}$$

where ε_y and ε_m are fiber and matrix strains, respectively, dx is a finite length between two consecutive nodes i and $i+1$ along the longitudinal x-axis. For typical low fiber volume fraction, the axial stiffness of the fiber A_yE_y is considerably lower than the matrix term A_mE_m and the contribution of matrix elongation to slip is ignored. Thus, the slip (s) and fiber strain ε_y are simplified to:

$$s = \int_{x_i}^{x_{i+1}} \varepsilon_y dx \quad \text{and} \quad \varepsilon_y = s' = \frac{ds}{dx} \tag{2}$$

The embedment length L is discretized into "n" nodes with equal spacing of h as shown in Fig. 6. The bond stress is assumed constant over the small spacing h for each node within each linear domain. Force in the fiber at the left end is imposed to be zero, simulating stress free condition, implying that the fiber strain or derivative of slip vanishes. At the right end the nodal slip is prescribed incrementally, simulating displacement control. As the loading progresses, the part of the fiber that slips out of the matrix has no frictional bond resistance; thus, fiber elongation is the only term in that section. The extruding part can be easily implemented by checking the amount of slip versus the embedment length of each node. If the slip is greater than the embedment length, zero bond stress is applied to that node.

A typical sisal pull-out force-slip curve is shown in Fig. 7a. Four distinct regions are indentified by roman numerals. Region I corresponds to the elastic-linear range with a rapid rate of ascent of the load. As the load increases beyond the linear region, a degree of nonlinearity is observed and this range is designated as region II which defines the initial point of fiber debonding. The peak response is reached at region III under partial debonding conditions, where the pull-out force reaches a maximum value (P_{au}). The slip (s) of the fiber at this point is defined as the slip at the peak and can be considered as the critical debonded length. For a given matrix and interface condition the peak pull-out force depends on the embedded length, diameter of the fiber and the curing period. The nominal shear strength computed at P_{au} is defined as the adhesional strength (τ_{au}). In region IV the load drops to a fixed value and remains constant thereafter. The pull-out behavior in the post-peak region is governed by the frictional shear strength of the interface and continues till the fiber is completely debonded from the interface. The shear strength at this region is defined as frictional resistant strength (τ_{fu}).

The adhesional and frictional components were quantified in terms of stress τ_{au} and τ_{fu}, respectively calculated using Soranakom

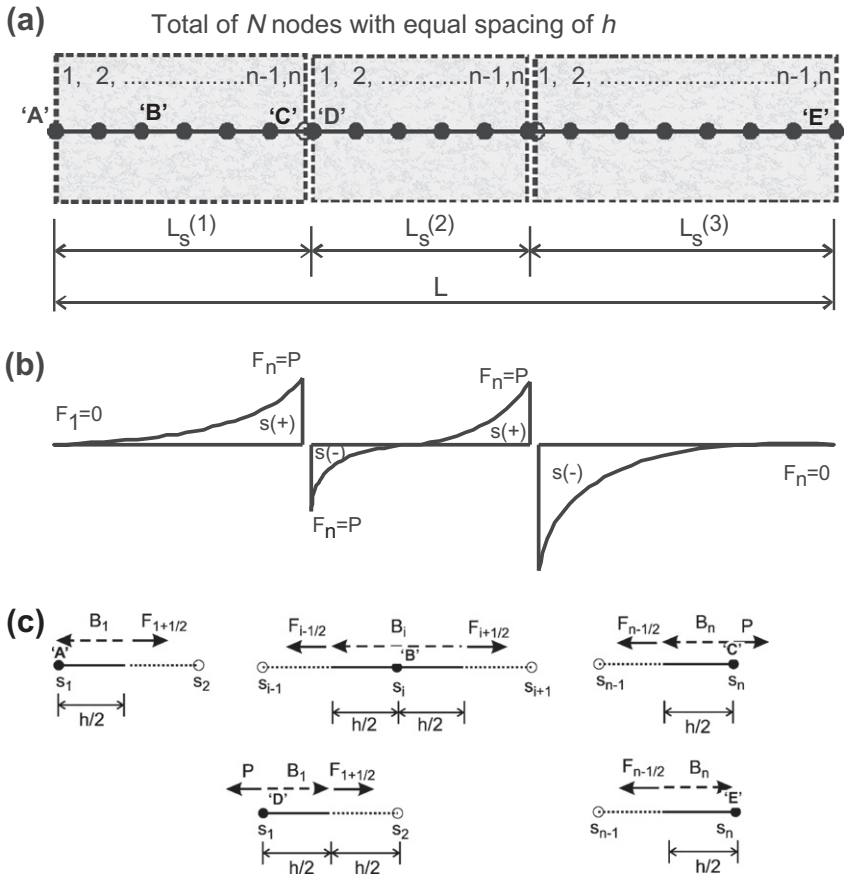

Fig. 6. Finite difference model: (a) discretized fiber pull-out model, (b) sign convention for slip and boundary conditions for force in fiber, and (c) free body diagram of five representative nodes labeled as "A"–"E".

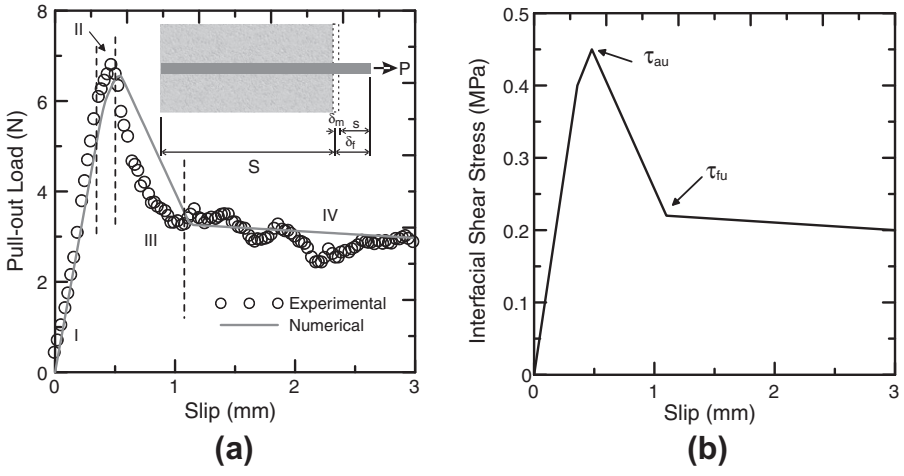

Fig. 7. Fiber pull-out test results of a sample tested after 3 days of curing with a embedded length of 20 mm: (a) comparison of the experimental and numerical result from the finite difference model and (b) interface constitutive relation obtained from the model.

and Mobasher's model [12]. The model correlation with experimental sisal fiber pull-out behavior can be seen in Fig. 7a. Using a back-calculation approach, the interfacial constitutive relation was determined from the model and presented in Fig. 7b. The points where the adhesional and frictional bond strength were calculated are indicated by arrows in the Fig. 7b.

Pull-out tests were carried out on embedded lengths of 10, 20, 30, and 40 mm after 3 days of curing and results are shown in Fig. 8. It was found that increasing the embedded length increased the pull-out force from 2 to 8 N. At an embedded length of 40 mm no significant increase was observed in the pull-out force related to adhesional and frictional bond. Note that the standard deviation of the fibers tested at 30 mm and 40 mm were essentially similar. The adhesional bond shear strength computed based on the Pull-out force using Soranakom and Mobasher model showed a constant value for the embedded lengths studied (see Table 1). As the

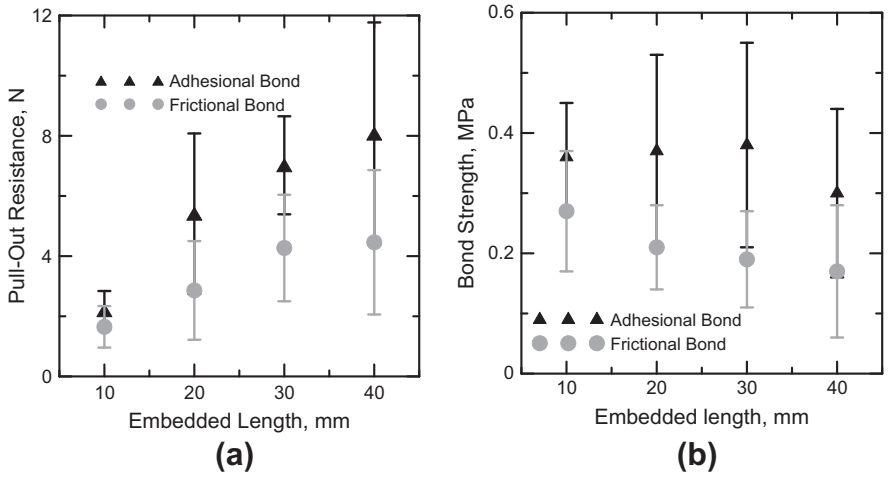

Fig. 8. Influence of embedded length on the fiber–matrix interfacial bond strength: (a) pull-out resistance increase with increasing embedded length and (b) bond strength does not improve when increasing embedded length.

Table 1
Summary of the results for pull-out samples tested with different embedment lengths. Values in parenthesis are standard deviation.

Embedded length (mm)	Type of fiber	P_{au} (N)	τ_{au} (MPa)	P_{au} (N)	τ_{fu} (MPa)	P_{au} average (N)	τ_{au} average (MPa)	P_{fu} average (N)	τ_{fu} average (MPa)
10	(i)	2.23 (0.18)	0.37 (0.01)	1.38 (0.51)	0.23 (0.08)	2.2 (0.64)	0.36 (0.09)	1.65 (0.69)	0.27 (0.10)
	(ii)	2.23 (0.64)	0.35 (0.09)	1.88 (0.62)	0.30 (0.09)				
	(iii)	–	–	–	–				
20	(i)	4.41 (2.49)	0.31 (0.15)	3.07 (1.23)	0.22 (0.15)	5.41 (2.67)	0.37 (0.16)	2.86 (1.64)	0.21 (0.07)
	(ii)	5.29 (2.78)	0.36 (0.21)	2.21 (0.98)	0.17 (0.07)				
	(iii)	7.06 (0.24)	0.45 (0.01)	3.21 (0.83)	0.23 (0.01)				
30	(i)	6.00 (1.87)	0.40 (0.19)	2.99 (1.90)	0.14 (0.09)	7.02 (1.63)	0.38 (0.17)	4.27 (1.77)	0.19 (0.08)
	(ii)	7.97 (1.77)	0.36 (0.11)	6.32 (2.07)	0.29 (0.09)				
	(iii)	7.14 (1.65)	0.38 (0.13)	4.03 (2.34)	0.15 (0.07)				
40	(i)	6.50 (2.40)	0.25 (0.10)	3.39 (1.99)	0.13 (0.09)	8.07 (3.7)	0.30 (0.14)	4.46 (2.4)	0.17 (0.11)
	(ii)	7.53 (3.98)	0.30 (0.15)	3.23 (2.72)	0.12 (0.08)				
	(iii)	9.49 (4.00)	0.34 (0.16)	6.00 (2.65)	0.23 (0.12)				

embedment lengths were increased, a slight decrease was observed in the measurement of frictional bond strengths. The present investigation is supported by similar conclusions for polypropylene and steel fibers found in the literature. Singh et al. [20] studied the pull-out behavior of polypropylene fibers from cementitious matrix for embedded lengths of 19, 25 and 38 mm. They found that despite the fact that the pull-out force increase with an increase in embedment length, the adhesional bond strength was found to be almost constant with a value around 0.5 MPa. Shannag et al. [21] investigated the pull-out behavior of steel fibers from cement composites for 6, 12, and 18 mm. They also found that by keeping other variables constant but increasing the embedded length from 6 to 18 mm a significant increase in the pull-out adhesional load was observed.

The effect of curing time from 3 to 28 days was investigated with results presented in Fig. 9. The bond strength reaches its maximum capacity at 14 days and the further curing of the matrix shows no effect on ages of 21 and 28 days (see Table 2). The average adhesional bond shear strength after 14 days ranged from 0.59 to 0.67 MPa. Individual values of adhesional bond shear strength at 14 days ranged from 0.35 to 1.29 MPa. Frictional bond shear strength results had less scatter with values ranging from 0.37 to 0.44 MPa after 14 days. The fiber–matrix bond shear strength results are in the range of some man-made fibers. Polypropylene fibers presented adhesional bond strength of 0.5 MPa [20].

The pull-out tests results were separated in terms of the fiber morphology. The sisal fiber can be divided in three types of mechanical bond components. Tables 1 and 2 show that different morphologies result in significant differences in the measured bond strength values. It is observed that fiber type (iii) with a characteristic of twisted arch shape resulted in the highest bond values. For example at 28 days of curing its adhesional bond shear strength was 0.92 MPa whereas fiber type (ii) and (i) presented values of 0.56 and 0.48 MPa, respectively. The influence on frictional bond was

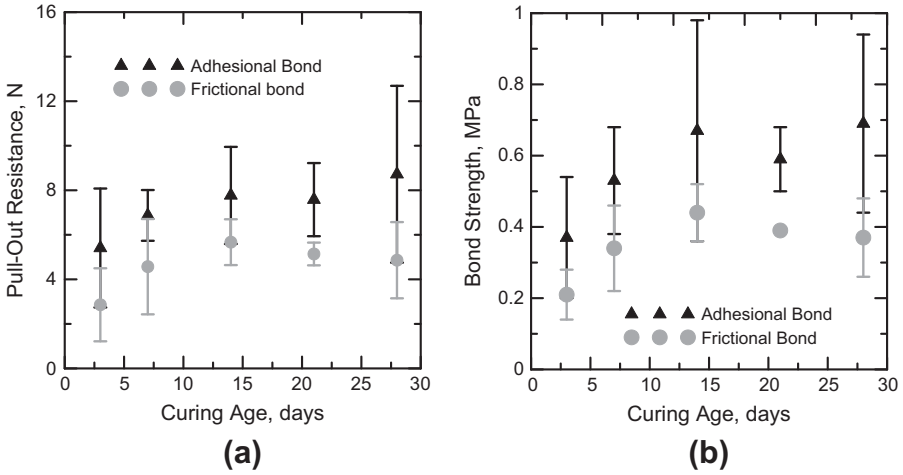

Fig. 9. Influence of curing age on the fiber–matrix interfacial bond strength. After 14 days there is no further increase in (a) pull out resistance and (b) bond strength.

Table 2
Summary of the results for pull-out samples tested at different curing time. Values in parenthesis are standard deviation.

Age (days)	Type of fiber	P_{au} (N)	τ_{au} (MPa)	P_{au} (N)	τ_{fu} (MPa)	P_{au} average (N)	τ_{au} average (MPa)	P_{fu} average (N)	τ_{fu} average (MPa)
3	(i)	4.41 (2.49)	0.31 (0.15)	3.07 (1.23)	0.22 (0.15)	5.41 (2.67)	0.37 (0.16)	2.86 (1.64)	0.21 (0.07)
	(ii)	5.29 (2.78)	0.36 (0.21)	2.21 (0.98)	0.17 (0.07)				
	(iii)	7.06 (0.24)	0.45 (0.01)	3.21 (0.83)	0.23 (0.01)				
7	(i)	5.46 (2.10)	0.47 (0.19)	3.38 (0.19)	0.29 (0.03)	6.87 (1.14)	0.52 (0.06)	4.57 (2.14)	0.34 (0.12)
	(ii)	8.34 (4.75)	0.59 (0.24)	7.04 (4.92)	0.48 (0.26)				
	(iii)	6.82 (1.05)	0.51 (0.07)	3.28 (1.43)	0.24 (0.10)				
14	(i)	6.64 (3.64)	0.52 (0.29)	5.06 (2.45)	0.35 (0.08)	7.77 (2.18)	0.62 (0.12)	5.67 (1.03)	0.44 (0.08)
	(ii)	6.3 (3.21)	0.58 (0.23)	5.10 (1.59)	0.46 (0.17)				
	(iii)	10.28 (5.03)	0.75 (0.34)	6.86 (3.21)	0.50 (0.20)				
21	(i)	–	–	–	–	7.58 (1.64)	0.59 (0.09)	5.14 (0.51)	0.39 (0.005)
	(ii)	7.06 (2.01)	0.51 (0.03)	5.51 (1.23)	0.40 (0.03)				
	(iii)	7.72 (1.86)	0.61 (0.09)	4.78 (0.50)	0.39 (0.01)				
28	(i)	5.54 (2.12)	0.48 (0.18)	2.31 (0.34)	0.20 (0.02)	8.72 (3.97)	0.67 (0.25)	4.86 (1.71)	0.37 (0.11)
	(ii)	7.01 (2.37)	0.56 (0.13)	5.57 (1.28)	0.46 (0.06)				
	(iii)	12.76 (1.71)	0.92 (0.12)	5.79 (0.29)	0.42 (0.01)				

not noticeable in the adhesion values. Fiber type (ii) shows higher values than type (i), especially in the curing age investigation.

The used models assume that the shape of the cross section remains virtually the same along the length, where as if there is any variation along the length of fiber, such variations will inherently result in additional anchorage. The influence of bond and fiber strength on the sisal fiber critical length was computed using an average shear strength approach. Fig. 10 correlates the sisal fiber critical length with its bond strength for a fiber radius of 0.1 mm and for several fiber ultimate tensile strengths (UTS). It can be seen that by decreasing the fiber strength the critical length proportionally decreases. The bond strength data (frictional and adhesional) are located in the fiber pull-out zone (see Fig. 10) and is not affected by the fiber embedment length. This behavior agrees with the composite idealized tensile behavior presented in Fig. 4 and with previous experimental data [1] characterized by a pull-out mechanism in the post-cracking zone.

Direct tensile tests were performed in long aligned sisal fiber reinforced cement composites with a volume fraction of 10%. An average UTS of 12 MPa was obtained with individual results ranging from 10.6 to 14.7 MPa. Multiple cracking in the form of an array of parallel distributed cracks orthogonal to the loading direction was observed with average final cracking spacing of 23 mm. This cracking pattern resulted in a tensile response with an ultimate strain of 1.53%. More information and details of the tensile behavior and cracking mechanisms of sisal fiber reinforced composites can be obtained elsewhere [1].

To simulate the tensile behavior of the sisal fiber reinforced composite a representation of the interfacial fiber–matrix and fiber model as shown in Fig. 11a was used. This interface model was obtained from a pull-out test performed on a fiber type (iii) with curing age of 3 days and embedded length of 20 mm (Fig. 7a). A fiber modulus of 19 GPa and UTS of 400 MPa was used as shown in

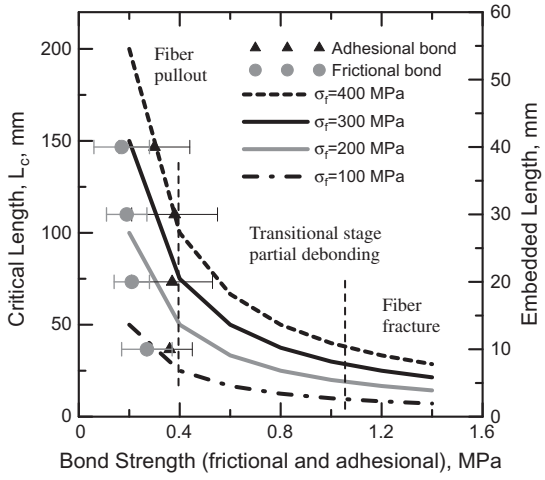

Fig. 10. Influence of bond strength and fiber strength on the fiber critical length.

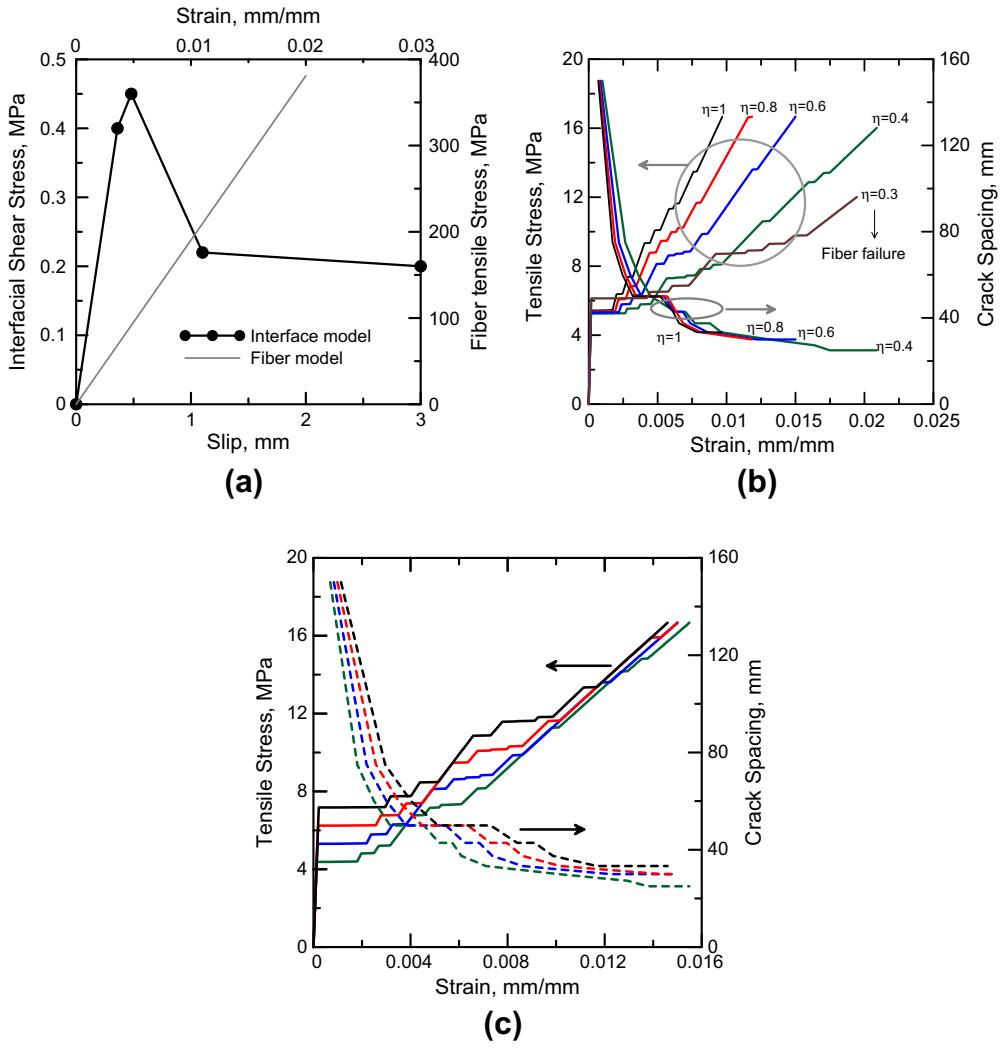

Fig. 11. Prediction of tensile response and crack spacing: (a) interface and fiber model used in the finite difference simulation, (b) effect of efficiency factor of fiber modulus and strength, and (c) effect of matrix first crack strength.

Fig. 11a. Matrix average tensile strength of 6 MPa and modulus of 35 GPa were selected. Since the fiber phase in the composite may not represent the same properties as those observed in a single fiber filament test, an efficiency factor (η) was defined to correlate the modulus and UTS of the fiber in both tests.

Fig. 11b shows the tensile response of sisal fiber reinforced cement composites and indicates that by decreasing the values of η, the total strain of the composite increases up to a point such that the fiber starts to fracture. An efficiency factor of 0.6 which presented ultimate strain of approximately 1.5% (based on experimental results) was selected. Note that the crack spacing also decreases when the parameter η, (representing the efficiency of the fiber stiffness) increases.

In a second step the influence of the matrix first crack strength on the tensile and crack spacing was investigated (see Fig. 11c). It is observed that a slight decrease in ultimate strain and increase in crack spacing occurs when the matrix first crack strength is increased. No effect on the UTS was noticed, indicating that the bond parameters are the dominant parameters in the tensile response of the continuous fiber composites.

Finally the influence of the fiber–matrix interfacial model was studied. A model that is presented in Fig. 12a and b obtained from a pull-out test at 21 days was used. This specific test resulted in higher adhesional and frictional bond strengths than the one previously used. Using an interfacial model with higher bond strength as the pull-out model results in a slight decrease in ultimate strain with little or no effect on crack spacing and UTS. It is hence clear that increasing the bond parameters directly improve the stiffness in the strain hardening portion of the curve.

Fig. 13 compares the experimental with predicted tension and crack spacing behavior. An efficiency factor η of 0.6, matrix first crack strength of 7 MPa and the interfacial bond model presented in Fig. 11a were used. An accurate correlation with the strain gage response is seen in the linear elastic region up to the first crack formation as shown in Fig. 13b. In the beginning of the multiple cracking zone, the model correlates well with a lower bound experimental curve up to a strain of 0.4%. After that point, the upper bound experimental curve overestimates the UTS. Numerical crack spacing values simulated show an accurate prediction up to a strain value of 0.005%. At the region corresponding to crack saturation, a crack spacing of approximately 30 mm is obtained which compares favorably with the 23 mm obtained from experimental results. The model has satisfactory predicted the crack spacing and tensile behavior which can be a useful tool for design purposes.

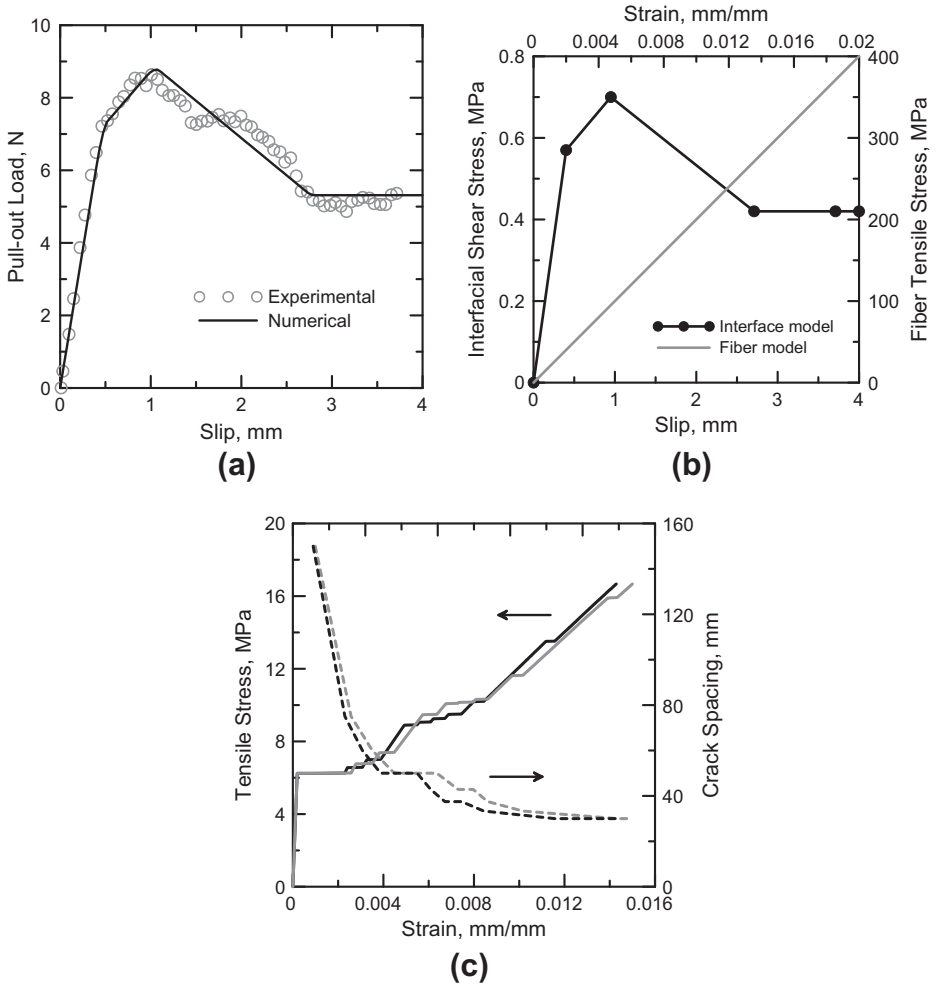

Fig. 12. Study on the effect of the interface model on the tensile response and crack spacing: (a) experimental and numerical pull-out response of a sample tested at 21 days of curing with an embedded length of 20 mm, (b) interface and fiber model used in the simulation, and (c) prediction of the composite tensile behavior and crack spacing.

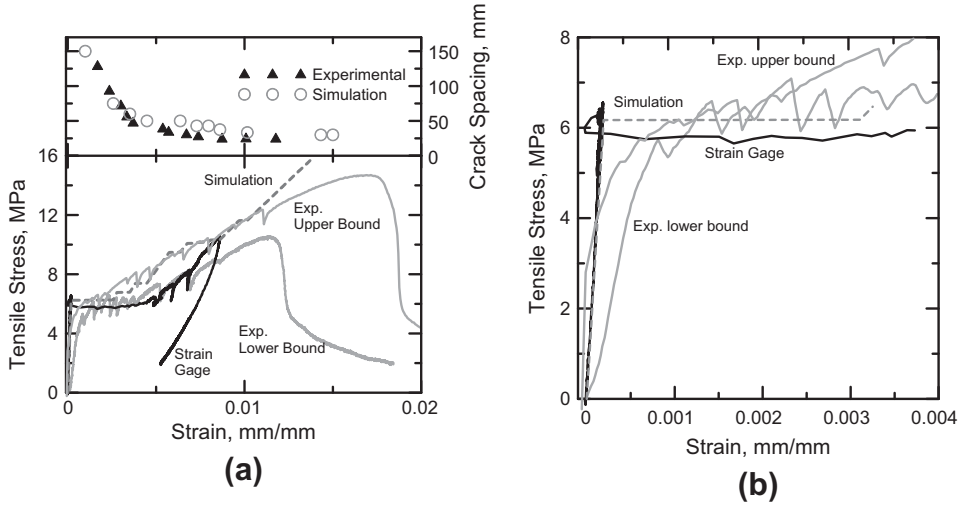

Fig. 13. Comparison of experimental and numerical results of the composite tensile response and crack spacing. (a) Two experimental tensile curves are shown: a lower and upper bound. (b) Numerical simulation shows a perfect fit with the strain gage response in the linear elastic range up to the first crack formation.

4. Conclusions

An investigation of the pull-out behavior of the sisal fiber from a cement matrix using the curing age, fiber morphology, and embedment length as variables was conducted. Results were evaluated using a finite difference model to determine the interfacial bond constitutive relation and to predict the continuous aligned sisal fiber reinforced composite tensile behavior in con-

junction with the crack spacing. The following conclusions can be drawn:

- It was observed that the sisal fiber morphology plays an important role in the bond strength. Three different cross-sectional geometries were reported: horse-shoe, arched and twisted arch shape. The highest values of bond stress were found for the twisted arch fiber type with an average adhesional and frictional bond strength of 0.92 and 0.42 MPa, respectively.
- The bond strength reaches its maximum capacity at 14 days and the further curing of the matrix shows no effect on ages of 21 and 28 days. Average adhesional bond for all three cross-sectional geometries strength after 14 days ranged from 0.59 to 0.67 MPa.
- It was found that the pull-out force increases as the embedded fiber length increases but no improvement in the bond shear strength was observed by increasing the embedded length from 10 to 40 mm.
- The bond strength of the sisal fibers with the used matrix (for a fiber volume fraction of 10%) resulted in a composite with a strain hardening behavior and multiple cracking formation under tensile loading and a failure mode characterized by a pull-out failure mechanism.
- The finite difference model can be applied to continuous aligned fiber reinforced composites. The model showed to be efficient for predicting the pull-out response of the sisal fiber from cement matrices. The simulation of the composite tensile response showed good correlation with the strain gage readings up to the first cracking strength. A good correlation with a lower bound experimental value up to a 0.4% strain was observed. After that point it fits the upper bound experimental curve overestimating the UTS. Model based final crack spacing values compare favorably with the experimental results.

Acknowledgements

The authors acknowledge Dr. Dallas Kingsbury (IMTL-ASU) for assisting with the set-up of the pull-out tests and Mr. Jeffrey Long (CEE-ASU) for helping in the production of the molds. This research was partially funded by CNPq (Brazilian National Science Agency).

References

[1] Silva FA, Mobasher B, Toledo Filho RD. Cracking mechanisms in durable sisal reinforced cement composites. Cem Concr Compos 2009;31:721–30.
[2] Silva FA, Mobasher B, Toledo Filho RD. Fatigue behavior of sisal fiber reinforced cement composites. Mater Sci Eng A 2010;527:5507–13.
[3] Silva FA, Zhu D, Mobasher B, Soranakom C, Toledo Filho RD. High speed tensile behavior of sisal fiber cement composites. Mater Sci Eng A 2010;527:544–52.
[4] Toledo Filho RD, Silva FA, Fairbairn EMR, Melo Filho JA. Durability of compression molded sisal fiber reinforced mortar laminates. Constr Build Mater 2009;23:2409–20.
[5] Naaman AE, Najm H. Bond–slip mechanisms of steel fibers in concrete. ACI Mater J 1991;88:135–45.
[6] Peled A, Bentur A. Quantitative description of the pull-out behavior of crimped yarns from cement matrix. J Mater Civil Eng 2003;15:537–44.
[7] Markovich I, Van Mier JGM, Walraven JC. Single fiber pullout from hybrid fiber reinforced concrete. Heron 2001;46:191–200.
[8] Kim DJ, El-Tawil S, Naaman A. Correlation between single fiber pullout and tensile response of FRC composites with high strength steel fiber. In: High performance reinforced cement composites (HPFRCC5); 2007. p. 67–76.
[9] Naaman AE, Namur GG, Alwan JM, Najm HS. Fiber pullout and bond slip I: analytical Study. J Struct Eng 1991;117:2769–90.
[10] Sueki S, Soranakom C, Mobasher B, Peled A. A pullout–slip response of fabrics embedded in a cement paste matrix. J Mater Civil Eng 2007;104:933–41.
[11] Banholzer B, Brameshuber W, Jung W. Analytical simulation of pull-out tests––the direct problem. Cem Concr Compos 2005;27:93–101.
[12] Soranakom C, Mobasher B. Geometrical and mechanical aspects of fabric bonding and pullout in cement composites. Mater Struct 2008;42:765–77.
[13] Soranakom C, Mobasher B. Modeling of tension stiffening in reinforced cement composites: part I – Theoretical modeling. Mater Struct 2010;43:1217–30.
[14] Soranakom C, Mobasher B. Modeling of tension stiffening in reinforced cement composites: part II – simulations vs. experimental results. Mater Struct 2010;43:1231–43.
[15] Silva FA, Chawla N, Toledo Filho RD. Tensile behavior of high performance natural (sisal) fibers. Compos Sci Technol 2008;68:3438–43.
[16] Silva FA, Chawla N, Toledo Filho RD. An experimental investigation of the fatigue behavior of sisal fibers. Mater Sci Eng A 2009;516:90–5.
[17] Silva FA, Chawla N, Toledo Filho RD. Mechanical behavior of natural sisal fibers. J Biobased Mater Bioenergy 2010;4:106–13.
[18] Silva FA, Toledo Filho RD, Melo Filho JA, Fairbairn EMR. Physical and mechanical properties of durable sisal fiber cement composites. Constr Build Mater 2010;24:777–85.
[19] Tonoli GHD, Santos SF, Savastano Jr H, Delvasto S, Mejía de Gutiérrez R, del M Lopez de Murphy M. Effects of natural weathering on microstructure and mineral composition of cementitious roofing tiles reinforced with fique fibre. Cem Concr Compos 2011;33(2):225–32.
[20] Singh S, Shukla A, Brown R. Pullout behavior of polypropylene fibers from cementitious matrix. Cem Concr Res 2004;34:1919–25.
[21] Shannag MJ, Brincker R, Hansen W. Pullout behavior of steel fibers from cement-based composites. Cem Concr Res 1997;27:925–36.